(This is a sample cover image for this issue. The actual cover is not yet available at this time.)

Biochimica et Biophysica Acta 1828 (2013) 471–478

Contents lists available at SciVerse ScienceDirect

Biochimica et Biophysica Acta

journal homepage: www.elsevier.com/locate/bbamem

Conductance properties of the inwardly rectifying channel, Kir3.2: Molecular and Brownian dynamics study

Tamsyn A. Hilder *, Shin-Ho Chung

Computational Biophysics Group, Research School of Biology, Australian National University, Canberra, ACT 0200, Australia

ARTICLE INFO

Article history:
Received 5 June 2012
Received in revised form 17 September 2012
Accepted 20 September 2012
Available online 27 September 2012

Keywords:
GIRK2
Kir3.2
Inwardly rectifying potassium channel
Conductance property
Molecular dynamics
Brownian dynamics

ABSTRACT

Using the recently unveiled crystal structure, and molecular and Brownian dynamics simulations, we elucidate several conductance properties of the inwardly rectifying potassium channel, Kir3.2, which is implicated in cardiac and neurological disorders. We show that the pore is closed by a hydrophobic gating mechanism similar to that observed in Kv1.2. Once open, potassium ions move into, but not out of, the cell. The asymmetrical current–voltage relationship arises from the lack of negatively charged residues at the narrow intracellular mouth of the channel. When four phenylalanine residues guarding the intracellular gate are mutated to glutamate residues, the channel no longer shows inward rectification. Inward rectification is restored in the mutant Kir3.2 when it becomes blocked by intracellular Mg^{2+}. Tertiapin, a polypeptide toxin isolated from the honey bee, is known to block several subtypes of the inwardly rectifying channels with differing affinities. We identify critical residues in the toxin and Kir3.2 for the formation of the stable complex. A lysine residue of tertiapin protrudes into the selectivity filter of Kir3.2, while two other basic residues of the toxin form hydrogen bonds with acidic residues located just outside the channel entrance. The depth of the potential of mean force encountered by tertiapin is −16.1 kT, thus indicating that the channel will be half-blocked by 0.4 μM of the toxin.

1. Introduction

The G protein-gated inwardly rectifying potassium channel, Kir3.2 (also known as GIRK2), selectively allows potassium ions to move more easily into, rather than out of, the cell [1]. Inwardly rectifying potassium (Kir) channels maintain the membrane resting potential, and regulate the action potential duration in electrically excitable cells [1]. Kir3.2, composed of 4 identical subunits, is present in the brain, pituitary and testis [2,3]. Abnormalities in G protein-gated inwardly rectifying potassium (GIRK) channel function have been linked to patho-physiology of neuropathic pain, drug addiction, cardiac arrhythmias, and other disorders [1,4]. In particular, Kir3.2 dysfunction has been implicated in seizure generation [1,5], atrial fibrillation, and the neurological symptoms seen in the weaver mice and other neuronal disorders [1]. Kir3.2 channels may provide a new target for the treatment of various neurological diseases such as epilepsy and Parkinson's disease [5,6].

Recently, the crystal structure of Kir3.2 has become available [2], creating an opportunity to computationally investigate several outstanding issues of its conductance properties. The first among these unresolved questions is the physical basis for inward rectification. The inward rectification observed in all Kir channels is thought to occur as a result of a combination of blockage of the channel by intracellular cations [1,5,7], such as Mg^{2+}, which block outward K^+ permeation by binding to residues in the transmembrane and cytoplasmic regions of the channel, and an unspecified intrinsic gating process [1]. However, studies of the cardiac I_{K1} inward rectifier K^+ channel have discounted block by divalent ions as the primary mechanism of rectification [8], and internal Mg^{2+} plays a minor part in the mechanism of rectification in endothelial cells [9]. It has also been proposed by Nishida and MacKinnon [10] that inward rectification is due to the amino acid composition of the cytoplasmic pore. Second, the structural changes that are required for the gating process are yet to be elucidated. The Kir3.x subfamily of channels is gated by G proteins. Upon stimulation by G proteins, the inner helix of the transmembrane domain is believed to swing away from the permeation pathway [1,11–13], thus rendering the constricted intracellular gate permeable to K^+ ions. The magnitude of such a displacement to cause the channel to transform from the closed to the open conformation, if it occurs, is not known. Third, the recognition mechanism involved in antagonist binding to the external vestibule of inwardly rectifying channels remains largely unexplored [4]. Although a number of drugs including anti-arrhythmia, anti-psychotic and anti-depressants block Kir channels, these intermediate-sized compounds tend to be non-selective and block the pores at relatively high concentrations [4]. There is, however, a 21-residue polypeptide

Abbreviations: Kir, Inwardly rectifying potassium channel; GIRK, G protein-gated inwardly rectifying potassium channel; TPN, Tertiapin; MD, molecular dynamics; BD, Brownian dynamics

* Corresponding author.
E-mail address: tamsyn.hilder@anu.edu.au (T.A. Hilder).

0005-2736/$ – see front matter © 2012 Elsevier B.V. All rights reserved.
http://dx.doi.org/10.1016/j.bbamem.2012.09.022

toxin, tertiapin (TPN) isolated from the honey bee, which blocks the pore of Kir channels with nanomolar to micromolar affinities, depending on channel subtype [3,14,15]. To develop more active and selective peptide blockers of inwardly rectifying channels it will be useful to identify first the important residue pairs for the binding of TPN to Kir3.2.

Few computational studies have been performed on Kir channels [16,17], and as far as we are aware none have investigated Kir3.2. Using several computational tools, we investigate the detailed processes by which K^+ ions move across Kir3.2, the structural basis for inward rectification, and the binding mode of TPN to the external entrance of the pore. We show that in its closed state the channel is devoid of water molecules along its cytoplasmic segment, which is lined with hydrophobic amino acid residues. A small expansion of the intracellular gate rapidly hydrates the pore and allows inward, but not outward, movement of K^+ ions. Replacement of four phenylalanine residues guarding the intracellular mouth with glutamate residues renders the channel open in both directions. The presence of Mg^{2+} in the intracellular space blocks outward currents in the mutant channel. Finally, we identify the key residues for the TPN–Kir3.2 recognition, and determine the potential of mean force encountered by TPN as it approaches the entrance of the channel. Our findings will further the understanding of inwardly rectifying channels and could lead to the development of targeted pharmaceuticals.

2. Computational methods

We obtain the coordinates of Kir3.2 from the protein database (PDB ID: 3SYA) [2]. As shown in Fig. 1, the Kir3.2 pore is made up of three distinct zones: the selectivity filter, located close to the extracellular side of the membrane is joined to a water cavity of 10–12 Å in diameter, and the pore then narrows towards the intracellular side of the membrane forming an intracellular gate.

First, we perform Brownian dynamics (BD) simulations to determine the conductance of ions through the channel. In BD simulations the total force acting on an ion at any discrete position in the channel, including the force resulting from induced surface charges on the protein wall, is calculated by solving Poisson's equation, as detailed elsewhere [18,19]. The dielectric constants of the protein and water within the pore are critical in calculating the correct force acting on the ion [20]. We use dielectric constants of 2 for the protein and 60 for the water within the pore, which have been shown to provide agreement to experimental data [21]. A schematic of the BD simulation system for the open channel is illustrated in Fig. 1. We place 7 K^+ and 7 Cl^- in each of the two cylindrical reservoirs 30 Å in radius to represent the intracellular and extracellular spaces. The height of the cylindrical simulation space is then adjusted to bring the ionic concentration to 140 mM. The simulation space is divided into two regions, a short time step region (2 fs) within the channel and a long time step region (100 fs) in the reservoirs. We run 5 simulations, each lasting 10 million time steps or 1 μs. We calculate the current using the relationship $I = qn/\Delta t$, where n is the average number of ions that cross the membrane, q is the charge of the ion, and Δt is the simulation time of one run.

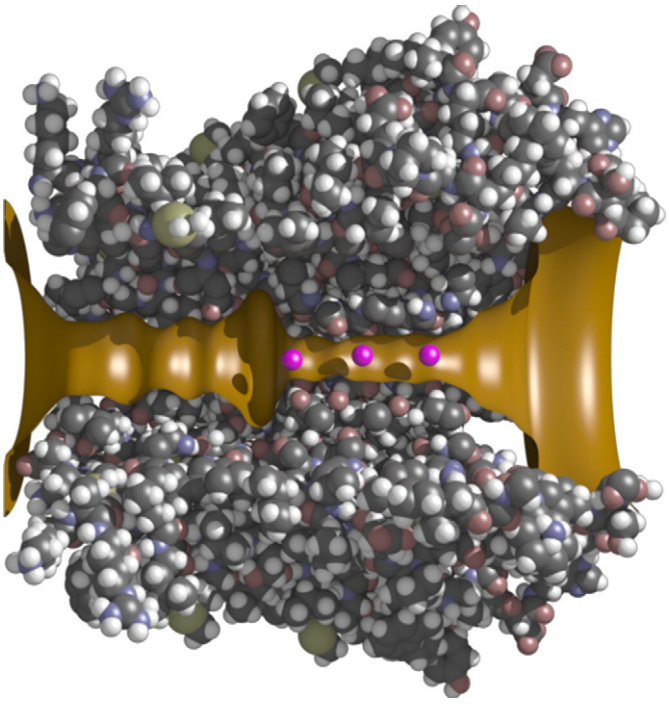

Fig. 1. Schematic representation of the Brownian dynamics simulation of Kir3.2: the atoms covering the top half of the pore were removed to reveal the channel conduit, shown in gold. Potassium ions are shown in pink. The intracellular side of the channel is on the left.

The crystal structure is found to be in the closed configuration since no potassium current is observed in BD simulations and no water molecules are present near the intracellular gate in molecular dynamics (MD) simulations. In a series of MD simulations using NAMD 2.8 [22] we gradually increase the radius of the intracellular gate by highly constrained minimization of the protein. In particular, we apply a large force radially outward on all atoms in the residues forming the gate. The intracellular gate at the bundle crossing region is progressively expanded until the channel becomes permeable to K^+ ions. A similar method has been used to open the selectivity filter of Kv1.2 channel [23]. To observe conduction it is necessary to increase the minimum radius of the entrance of the inner gate from 1.6 Å to 3.4 Å. This expansion compares reasonably with the work of Whorton and MacKinnon [2]. They found that a R201A mutation caused the inner helix gate radius of the GIRK2 channel to expand to 5.5 Å and caused the channel to remain in the open conformation [2]. A similar movement of the inner helix is believed to occur in KirBac1.1 when activated by G-protein [11]. This expansion is illustrated in Fig. 3A. We also perform BD simulations to investigate the effect of mutating the bulky phenylalanine residue at the bundle-crossing region (F192) in the closed structure to a glutamic acid residue, and adding 4 Mg^{2+} ions to the intracellular reservoir of the mutated structure. Detailed descriptions of BD simulations are given in Hoyles et al. [24]. We assign the full charge of ± 1 e to all ionizable residues in the channel protein. Reducing the charges on these residues may influence the depth of the electrostatic energy. Based on free energy changes associated with moving a residue from an aqueous to a protein environment, Ranatunga et al. [25] calculated absolute pKa values of all ionizable residues in the crystal structure of KcsA. Free energies in their study were estimated by solving the linearized Poisson–Boltzmann equation. They showed that the ionization states of most side chains at neutral pH remained close to their default states, except two residues (R64 and E71) near the extracellular entrance to the channel. Subsequently, Burykin et al. [26] carried out similar calculations, based on a more rigorous and self-consistent method. Their estimates of pKa values of ionizable side chains were obtained by using the so-called 'protein-dipole-Langevin-dipole' model. It is also possible to derive protein pKa values based on first principles, such as QM/MM calculations [27,28], although such calculations are computationally expensive and are therefore less common. In the preliminary study we report here, we use the default ionization states of all polarizable side chains in Kir3.2. The use of their optimal ionization states at neutral pH, which may differ slightly from those of the default states, may have an effect on the energetics of ion permeation. Such a comparison will be the subject of our future study.

MD simulations are used to determine the bound configuration of TPN and calculate the profile of potential of mean force (PMF) of TPN binding to the channel. All MD simulations are performed using NAMD 2.8 [22] and visualized using VMD 1.9 [29]. Throughout, we

use the CHARMM36 force field [30,31], and TIP3P water, with a time step of 2 fs, at constant pressure (1 atm) and temperature (310 K). The Kir3.2 channel and Kir3.2–TPN complex are embedded in a 3-palmitoyl-2-oleoyl-D-glycero-1-phosphatidylcholine (POPC) lipid bilayer, solvated in a $100\times100\times104$ Å^3 box of water. Potassium and chloride ions are added both to neutralize the system and simulate a 200 mM ionic concentration. The switch and cutoff distances are set to 8 and 12 Å, respectively. The protein is initially held fixed, allowing the water and ions to equilibrate during the simulation period of 5 ns, and in subsequent simulations the protein and lipid bilayer centers of mass are held by a harmonic constraint of 0.2 kcal/mol/Å^2. A similar methodology was used in simulations on Kv1.3 [32].

We obtain the coordinates of TPN from the protein database (PDB ID: 1TER) [33]. To determine an initial starting configuration of the bound TPN–Kir3.2 structure we use the rigid-body docking program ZDOCK 3.0.1 [34]. The top-ranked 600 structures are considered as possible docking modes. Using our knowledge of toxin binding to other biological potassium ion channels [23,32] we search the docked structures for candidates where one of the lysine residues (either 16, 17, 20 or 21) are docked into the selectivity filter. The lysine residue at position 17 is docked into the selectivity filter in 6 of the top-ranked structures and no other lysine residues are observed to dock into the selectivity filter. The arginine residue at position 7 and histidine residue at position 12 are shown to occlude the entrance to the pore in 2 of the top-ranked structures, but no other top-ranked structures are shown to protrude into the selectivity filter. The flexibility of the toxin and the protein is not taken into account in ZDOCK. Therefore, we perform MD simulations to determine the predicted bound state. We use the highest ranked docked structure as the starting configuration in MD simulations. We examine the binding of TPN using the docked structure with the lysine 17 protruding into the filter since it is the highest ranked and most common of the docked structures.

The PMF for the binding of TPN to Kir3.2 is determined using umbrella sampling. Using the equilibrated Kir3.2–TPN structure from MD simulations we generate sampling windows by performing steered MD. A force of 30 kcal/mol/Å is applied to pull TPN out of the binding site. During the steered MD simulation the backbone atoms of the protein are held fixed and a harmonic constraint of 0.2 kcal/mol/Å^2 is applied to the backbone atoms of TPN to maintain the root-mean-square deviation, with reference to a starting structure below 0.5 Å so that no significant distortion of the structure occurs. The channel central axis (z-axis) is used as the reaction coordinate. The pulling generates a continuous number of configurations along the permeation pathway so that we can construct umbrella sampling windows every 0.5 Å.

During umbrella sampling the center of mass of the backbone atoms of TPN is confined to be within a cylinder of 8 Å centered on the channel axis, and beyond this a harmonic potential of 20 kcal/mol/Å^2 is applied. This is shown to provide adequate sampling. Moreover, a force constant of 30 kcal/mol/Å^2 is applied in the z direction to constrain the center of mass of TPN to the sampling window. The center of mass coordinates of the backbone atoms of TPN is saved every 0.5 ps. The PMF is then constructed along the z direction using the weighted histogram analysis method [35] and the center of mass coordinates. Each sampling window is run for 5 ns. The PMF is shown to converge as the depth changes by less than 0.5 kT when simulations are run for a further 1 ns. These simulation times also compare well with other work on potassium channels [23,32,36].

The dissociation constant (K_d) in the unit of molar is estimated to be [32,37]

$$K_d^{-1} = 1000 N_A \pi R^2 \int_{z_1}^{z_2} \exp(-W(z)/k_B T) dz, \quad (1)$$

where $W(z)$ is the 1D PMF with the zero point located at bulk, $1000N_A$ is used to convert from m^3 to L/mol, k_B and T are Boltzmann's constant and temperature respectively, z_1 is in the binding pocket and z_2 is in the bulk [36]. Although Eq. (1) was originally derived for the binding of an ion to the channel [37] it has also been successfully applied to toxin binding of Kv1.3 [32], Kv1.2 [23] and KcsA [36]. Note that the window at 45.5 Å is assumed to be bulk and the PMF is therefore set to zero at this z position. TPN is docked to Kir3.2 at $z=19.0$ Å and the center of mass of Kir3.2 is located at $z=0$ Å. A hydrogen bond is assumed to be formed if the donor–acceptor distance is within 3.0 Å and the donor–hydrogen–acceptor angle is $\geq$150 [32]. A salt bridge is formed between TPN and Kir3.2 if the distance between any of the nitrogen atoms of a basic residue on TPN and the oxygen atoms of an acidic residue on Kir3.2 is $<$4 Å [32]. The approach described above to determine the binding free energy of TPN has been successfully applied to a number of other channel–toxin interactions [23,32,36,38]. It is also possible to study the binding of toxins using the linear interaction energy (LIE) method and free energy perturbation (FEP) such as in [39,40]. Whether or not these two methods can be reliably applied for studying the binding of large polypeptide toxins to a channel protein remain to be investigated. There are two main disadvantages for estimating the free energy for toxin–channel binding using MD. First, it is computationally expensive to construct a PMF using the umbrella sampling method. Typically, it takes between 50,000 and 75,000 CPU hours of a modern supercomputer to construct a PMF of one toxin. Second, since simulations can only be run for a relatively short time, usually about 5–10 ns, it is not possible to ascertain whether or not a PMF has converged or will drift to another value if simulations are continued for additional tens or hundreds of nanoseconds.

3. Results

3.1. Hydrophobic gating and ion conduction

The crystal structure obtained from Whorton et al. [2] is in the closed configuration and no potassium current is observed in BD simulations, despite there being an unobstructed pathway through the pore.

The intracellular gate runs from the internal water cavity to the intracellular mouth of the channel ($z=-26$ to -10 Å) with a minimum radius of 1.58 Å. This region of the channel is surrounded by hydrophobic residues, such as alanine, valine, methionine and phenylalanine. In MD simulations of the closed channel water molecules are not present in this region, but when this region is expanded water floods into the pore, as shown in Fig. 2. This expansion could represent the TM2 helix swinging away from the permeation pathway upon G-protein activation as mentioned by a number of authors [1,11,13]. In mutagenesis studies, Yi and colleagues [13] found that the Kir3.2 transmembrane domain undergoes substantial rotation as the channel opens and closes, and that gating is likely to involve more than one gate. In our Kir3.2 model the glycine hinge (G180) discussed by Hibino et al. [1] is located at -8 Å and approximately coincides with the start of the hydrophobic region of the pore, and where we begin to expand the channel. Our results suggest that the pore is gated by a "hydrophobic gating" mechanism also reported for the Kv1.2 and acetylcholine receptor channels [41,42]. It has also been suggested by Dryga et al. [43] that the gating of Kv1.2 is electrostatic gating which occurs due to the movement of positive gating charges in response to the applied potential, which in turn allow attached non-polar regions to open and close.

By expanding the intracellular gate, as illustrated in Fig. 3A, the channel is transformed into the open configuration and potassium currents are measured in BD simulations. From BD simulations, a potassium ion entering the Kir3.2 wild-type open channel encounters a large energy well of 56 kT, created by polar and charged residues lining the protein wall, as shown in Fig. 3B. The magnitude of the well depth compares well with some studies on potassium channels. For example, for KcsA the depth of the potential energy encountered by a single ion traversing across the pore is approximately 60 kT within

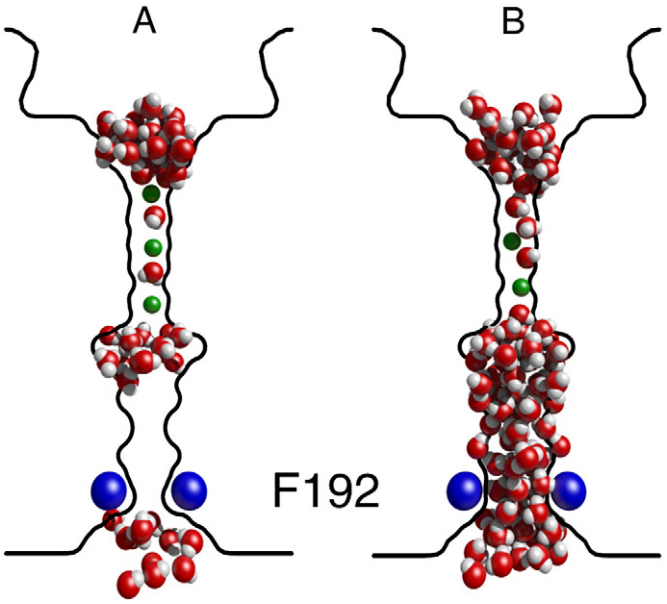

Fig. 2. Illustration of hydrophobic gating. Snapshots of water molecules and potassium ions (shown in green) in the channel conduit are obtained during molecular dynamics simulations from the closed (A) and open (B) channels. The bulky phenylalanine residue (F192) at the bundle crossing region is shown in blue. For clarity only the pore outline from BD simulations is shown, and water is shown if $-30<z<20$ Å.

the selectivity filter with respect to the reservoir [19,44]. The well is deep enough to attract 3 K^+ ions; in the absence of an applied electric field, there are, on average, 1.5 ions in the selectivity filter, and 1.5 ions in the water cavity between −10 and −3 Å. As shown in the histogram (Fig. 3C), the three regions where ions dwell preferentially are located at $z=-6.5$ (inside the cavity), −1 (near the T154 carbonyl oxygen) and +4 Å (near the I155 carbonyl oxygen). Also there is another prominent peak at 23 Å, near the external mouth of the channel. No ions reside in the intracellular hydrophobic gate region of the channel.

In Kir3.2 a bulky hydrophobic phenylalanine residue at position 192 is located at the mouth of the intracellular gate (see Fig. 2). The F192 residue has previously been suggested as a contributor to the gating of Kir3.2 [1]. Moreover, the KirBac1.1 [11] and Kir3.1/Kir3.4 [12] channels are also blocked by a bulky phenylalanine residue. Replacement of these residues in Kir3.1/Kir3.4 to smaller alanine residues converted the channel to the open state [12]. By making the mutation F192E to the closed Kir3.2 channel we are also able to convert the channel to the open state. Similar to the expanded pore, in MD simulations, the hydrophobic region becomes fully hydrated in the F192E mutant channel.

3.2. Inwardly rectifying current–voltage relationships

We study the conductance properties of the channel under various conditions by performing BD simulations. The current–voltage curve for the open-state, wild-type channel, and a mutant channel with or without Mg^{2+} in the intracellular reservoir are shown in Fig. 4. The wild-type open channel exhibits inward rectification in the absence of divalent cations (Fig. 4A). The curve constructed with the symmetrical concentration of 140 mM KCl under various applied potentials is pronouncedly nonlinear. The currents at 100 mV and −150 mV are 0.4 ± 0.2 pA and -6.9 ± 0.6 pA, respectively. The potassium conductance varies from 14 pS at −100 mV to 45 pS at −150 mV. This compares well with experimentally-determined values of the single-channel conductance of Kir3.2 and related isoforms [3,45]. Kubo et al. [3] reported potassium conductances of 30 pS in 150 mM symmetric K^+ and 32 pS in 140 mM symmetric K^+ for the isoforms Kir3.2c and Kir3.2d, respectively.

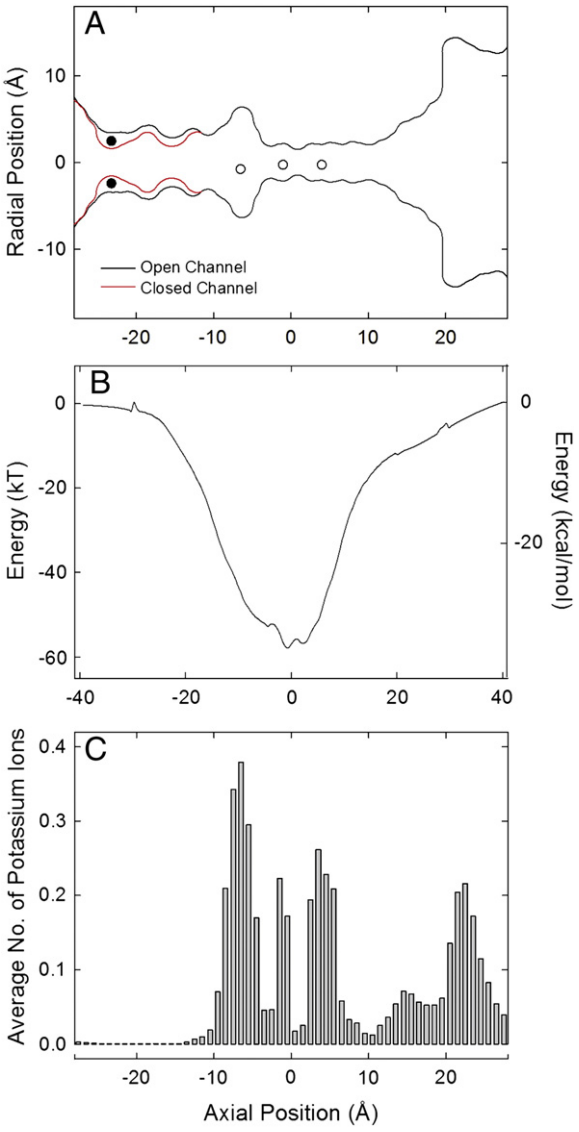

Fig. 3. The pore outline, energy profile and dwell histogram of Kir3.2 obtained from Brownian dynamics simulations. (A) The outline of the pore in the closed state, derived from the crystal structure, is shown in red. The intracellular gate of the channel is expanded to allow K^+ ions to move across, as shown in solid black lines. For clarity, the ordinate of the graph is expanded. The filled circles indicate the position of the bulky phenylalanine residue (F192) and open circles indicate the position of potassium ions. (B) Electrostatic energy profile of a potassium ion traversing the open-state of the channel along the central axis is calculated at 0.5 Å intervals. (C) To obtain the dwell histogram, the channel is divided into 100 thin sections, and the number of ions present in each section over a simulation period of 1 μs is tabulated. (For interpretation of the references to color in this figure legend, the reader is referred to the web version of this article.)

Similarly, Kofuji et al. [45] determined a mean single-channel conductance for Kir3.2 of 30 ± 2 pS over the range of −40 to −100 mV. We add 4 Mg^{2+} ions to the intracellular reservoir of the wild-type open channel. The residual outward current is completely blocked by the addition of intracellular Mg^{2+}.

One possible reason for the attenuation of the outward current, as seen in Fig. 4A, may be due to the lack of acidic residues guarding the intracellular gate. In KcsA, there are four acidic residues (E118) in the region occupied by four hydrophobic phenylalanine residues (F192) in Kir3.2. The presence of the acidic residues near the intracellular gate of KcsA creates a deep attractive energy well for K^+ ions, thus facilitating the outward conduction under the influence of an applied potential [18]. When the charges on the four acidic residues of KcsA were removed the channel became inwardly rectifying [46]. By

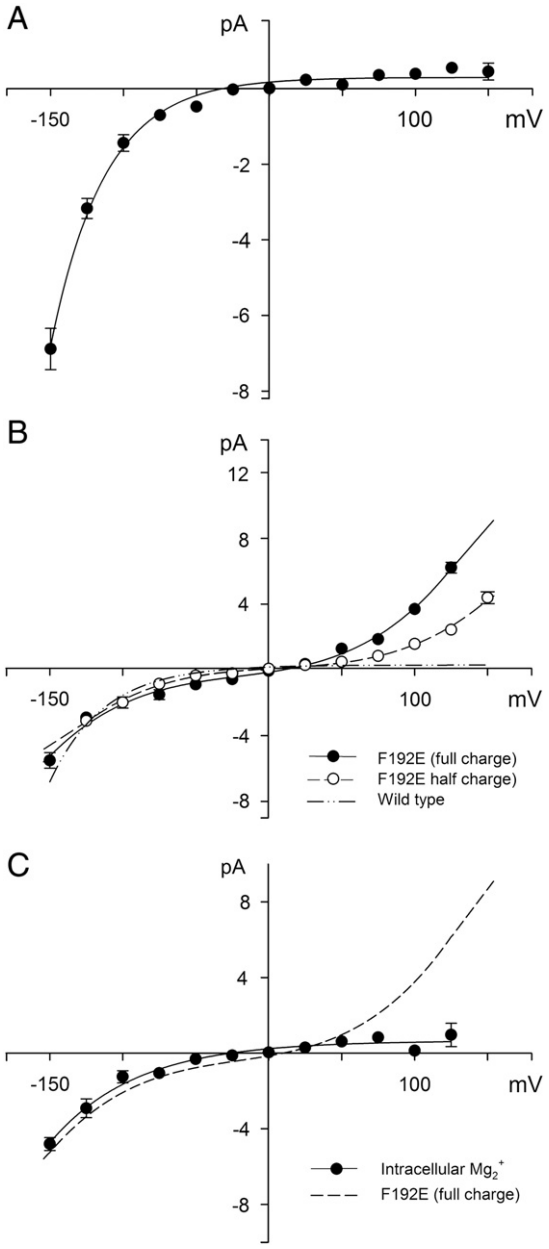

Fig. 4. Current–voltage profiles derived from Brownian dynamics simulations. (A) The profile is obtained from the wild-type Kir3.2 channel in the open state with symmetrical solutions of 140 mM KCl in both reservoirs. (B) The profile is obtained from a mutant channel in which four phenylalanine residues at position 192 in the wild-type channel in the closed state are replaced with glutamate residues. (C) Using the same F192E mutant channel as in (B), the profile is obtained after adding 4 Mg^{2+} in the intracellular reservoir. Each data point represents the average of five sets of simulation, each simulations lasting 10 million time steps (1 μs). Error bars represent one standard error of the mean, and error bars smaller than the data points are not shown.

examining the F192E mutant channel we can investigate if the outward current can be magnified by creating an energy well near the intracellular entrance of the pore. The current–voltage relationship of the F192E mutant is not inwardly rectifying, as shown in Fig. 4B. The potassium current is 3.7 ± 0.25 and -2.0 ± 0.34 at ± 100 mV. The F192E mutation results in the four negatively charged glutamic acid residues located in close proximity to each other and consequently it is likely that some of these residues would protonate. We investigate the effect of protonation by reducing the charge on each Glu residue by half, which is roughly equivalent to assuming that two of the residues are protonated. Although this is a first approximation which may affect short-range electrostatic interactions with the ions, it provides insight as to the conduction mechanisms. No inward rectification is observed using only half the partial charges on the F192E mutation (Fig. 4B). For comparison, the current–voltage relationship obtained for the open wild-type channel is reproduced here from Fig. 4A (dash-dot line). Our results suggest that inward rectification is due to the lack of negatively charged residues at the intracellular mouth of the channel, combined with the small entrance encountered by potassium ions. The F192 residue constricts the intracellular entrance to the pore, thereby reducing the probability of a potassium ion entering from this direction.

A number of studies have proposed that inward rectification in Kir3.2 channels is due to the presence of intracellular cations, such as Mg^{2+} [1,5,7]. We investigate this prediction by adding 4 Mg^{2+} ions to the intracellular reservoir of our F192E mutant channel. The addition of intracellular Mg^{2+} generates an inwardly rectifying potassium current, as shown in Fig. 4C. For comparison, the current–voltage relationship obtained from the F192E mutant channel without Mg^{2+} is reproduced here from Fig. 4B (broken line). On average 1 Mg^{2+} ion is located in the selectivity filter (at approximately 3.5 Å) at an applied potential of 100 mV, and 0.2 Mg^{2+} ions are located in the water cavity (at approximately −8 Å) at an applied potential of −100 mV. In other words, at a positive applied potential Mg^{2+} enters the channel and blocks outward current of the F192E mutant, thereby making the channel inwardly rectifying.

3.3. Binding of tertiapin (TPN)

A short peptide from honey bee venoms, tertiapin, whose structure is shown in Fig. 5A, inhibits certain types of Kir channels with nanomolar to micromolar affinities. The ellipsoidal polypeptide toxin carries the net charge of +6 e (one histidine, one arginine and four lysines). The bound state of TPN after molecular docking and 3.2 ns MD simulations is shown in Fig. 5B. In accord with the report by Kitamura et al. [15], TPN binds to the extracellular side of Kir3.2. A lysine residue (K17) protrudes into the channel selectivity filter. Although there are presently no experimental results available detailing the binding of TPN to Kir3.2 our results compare well with Jin et al. [47] who examined the binding of TPN-Q (a derivative of TPN with the methionine residue at position 13 mutated to glutamine) to the Kir1.1 channel (ROMK1). They found that a much higher concentration of TPN-Q was required to inhibit half the current when Lys17 was mutated to alanine [47].

To verify the predicted binding of TPN to the channel we determine the PMF for the unbinding of TPN from the channel, as shown in Fig. 6. The PMF reaches a minimum at 19.0 Å, where the channel center of mass is at 0 Å. The PMF increases from −16.1 kT at 19.0 Å to −5.0 kT at 25.0 Å. It is assumed that the properties for the window at $z =$ 45.5 Å are similar to bulk, and therefore the PMF is set to zero at this point. As TPN moves away from its bound state at the selectivity filter it interacts with the side chains of the extracellular vestibule and as a result the PMF gradually increases from −5.0 kT at 25.0 Å to bulk at 45.5 Å. We find that the bonds between TPN and Kir3.2 become stable after the first 1 ns of umbrella sampling. Therefore, the first 1 ns of umbrella sampling is considered equilibration. After 1 ns, and for the remainder of the simulation, the residue pair Lys21–Asp164 forms a salt bridge between TPN and Kir3.2, as shown in Fig. 5. Jin at al. [47] also showed that mutating Lys21 to alanine in Kir1.1 requires a much higher concentration of TPN-Q. In our simulations we used particle mesh Ewald electrostatics and a non-polarizable force field which have been shown to effect the free energy [20,48].

Using Eq. (1) we obtain a dissociation constant, K_d of 0.4 μM. At present only one quoted value for the binding affinity of TPN to Kir3.2 is available in the literature. Kubo et al. [3] quoted an unpublished IC_{50} of 7 nM for the Kir3.2d isoform. TPN binds to Kir channels with varying affinity. For example, TPN binds to Kir1.1 and the heteromeric Kir3.1/Kir3.4 channels with high affinity ($K_d = 1.3$–2 nM and 8–10 nM, respectively)

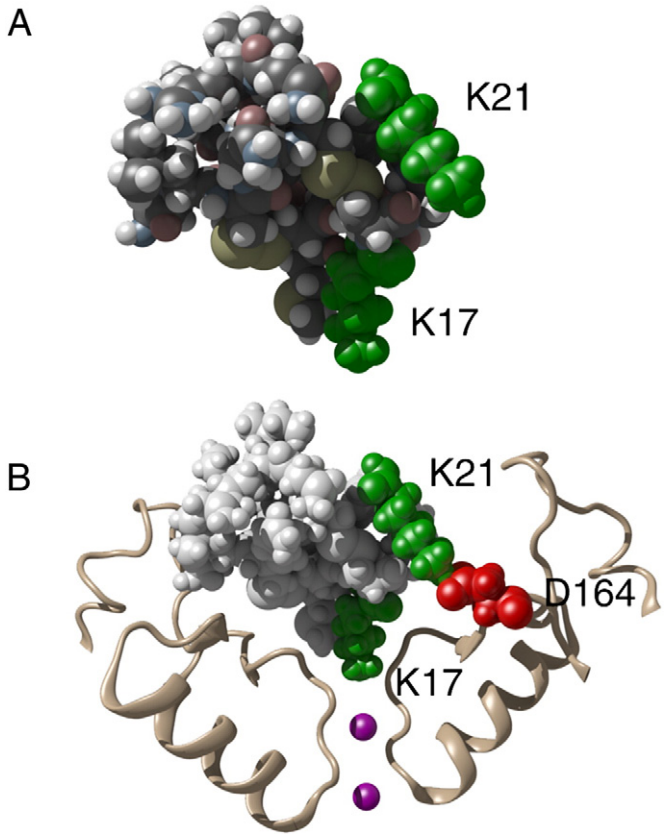

Fig. 5. Binding of tertiapin (TPN) to the outer vestibule of Kir3.2. (A) Illustration of TPN and (B) TPN bound to Kir3.2. Lysine residues (K17 and K21) are highlighted in green. In (B) residue K17 points into the selectivity filter. Residue K21 is bound to D164 residue (shown in red) of Kir3.2. For clarity only part of the channel is shown. Two potassium ions in the selectivity filter are shown in pink.

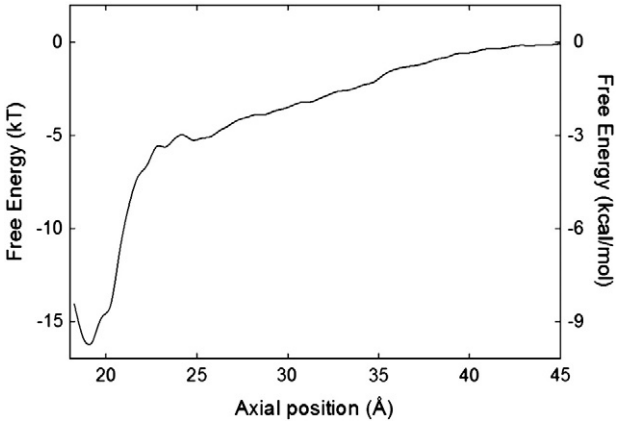

Fig. 6. Potential of mean force encountered by tertiapin (TPN). The profile of PMF for the unbinding of TPN is constructed with molecular dynamics. The axial position represents the distance in the *z*-direction from the center of mass of the channel.

[14,15,49,50], but Kir2.1 is relatively insensitive to TPN ($K_d = 20$ μM) [14,15].

To characterize the interactions between TPN and Kir3.2 we analyze the non-bonded interaction energy, hydrogen bonding and salt bridge formation for the umbrella sampling window at $z = 19.0$ Å, which corresponds to the minimum of the PMF profile shown in Fig. 6. The interaction energies are determined using the NAMD Energy Plugin [22] without particle mesh Ewald (PME), and the system's overall net charge is 0. These interaction energies do not represent the relative free energy between toxin–channel residues but merely provide insight into the electrostatics and strength of the interaction between TPN and Kir3.2 in the bound configuration. To determine the free energy of these toxin–channel interactions would require mutation of the proteins to a neutral residue using FEP. We note that again the first 1 ns of the trajectory is considered equilibration and is excluded from the analysis. The electrostatic and van der Waals (or non-bonded) interaction energy between TPN and the channel are -343 ± 22 kcal/mol and -57 ± 5 kcal/mol, respectively. The electrostatic energy is approximately 6 times higher than the van der Waals energy. We can get a sense of the stability of the bound configuration by comparing to the interaction energy between TPN and the channel for the windows at $z = 25.0$ and 45.5 Å. The electrostatic and van der Waals interaction energy between TPN and the channel are -205 ± 68 kcal/mol and -17 ± 5 kcal/mol respectively at 25.0 Å, and -0.19 ± 0.69 kcal/mol and -0.01 ± 0.02 kcal/mol at 45.5 Å respectively.

We determine the average number of hydrogen bonds and electrostatic interaction energy (at window 19.0 Å) which form between the most important TPN–Kir3.2 residue pairs. Each value represents the average of 400 frames (the first ns of the simulation is ignored), and standard deviations are given. The residue pair Lys17–Tyr157 forms on average 1.5 ± 0.6 hydrogen bonds with an electrostatic interaction energy of -77.9 ± 4.0 kcal/mol. The residue pair Lys21–Asp164 forms on average 0.8 ± 0.4 hydrogen bonds with an electrostatic interaction energy of -94.6 ± 9.2 kcal/mol. The magnitude of these electrostatic interaction energies compares well with those determined for the binding of ShK to the voltage-gated potassium channel Kv1.3 [32]. Comparing these electrostatic energies with those at 21.0 Å, in other words moving in the *z*-direction away from the minimum energy position, we obtain an electrostatic interaction energy of -64.4 ± 6.9 kcal/mol and -7.0 ± 8.5 kcal/mol for the Lys17–Tyr157 and Lys21–Asp164 residue pairs, respectively. At 25.0 Å, where the PMF begins to flatten, these values decrease further to -2.4 ± 2.6 kcal/mol and -0.7 ± 1.9 kcal/mol for the Lys17–Tyr157 and Lys21–Asp164 residue pairs, respectively. This further illustrates the relative stability of the bound configuration. The salt bridge formed between Lys17–Tyr157 residue pair is broken at 22.0 Å.

4. Discussion

In several BD studies by Chung and colleagues [18,19,23,44] the forces acting on the ions are calculated by solving Poisson's equation with the dielectric constant of the water $\varepsilon_w = 60$ and the protein $\varepsilon_p = 2$. Compared to the energy profile estimated using these values of dielectric constants, Burykin et al. [26,51] obtain a significantly shallower well for KcsA. In their work, MD simulations are used to sample thermodynamic ensembles of protein coordinates, for the purpose of computing the electrostatic self energy of ions using the protein-dipole-Langevin-dipole model in its linear response approximation. In this model, the linear response of dipoles in the protein to the presence of the ion is explicitly taken into account, while water is represented as a combination of explicit water molecules, Langevin dipoles, and a dielectric continuum to represent the boundary conditions. This energy profile is then used in subsequent BD simulations using CHANNELIX to determine ionic conductance [51]. Therefore, in their work the dielectric properties of the protein are largely represented explicitly by mobile protein dipoles, while a low dielectric constant of 4 is used to represent residual effects. The study revealed, for example, that the pore is occupied by one ion in the selectivity filter, and the second ion entering the pore causes the resident ion to move out of the filter, with conduction thus occurring by a two-ion knock-on mechanism. In BD studies by Chung et al. [18], the selectivity filter is occupied by two ions and conduction takes place when a third ion entering the selectivity filter disrupts the stable equilibrium established by the two resident ions. Allen et al. [19] also confirmed this 3-ion conduction process by MD studies.

In this study also, we use the value of 2 and 60 for the dielectric constants of the protein ε_p and the water in the pore ε_w to determine the force acting on an ion by solving Poisson's equation. Unlike water and lipid, proteins exhibit large variations in polarizability depending on the location [52]. Thus, in a macroscopic point of view, one should assign varying values of ε_p, a high value near the water–protein interface and a low value in the deep interior of the protein. In practice, assigning a fixed value to an entire protein in continuum electrostatic calculations appears to work well. Chung et al. [18] used $\varepsilon_p = 3.5$ and 5 in solving Poisson's equation and compared the results of BD simulations obtained by using these values to those obtained by assuming $\varepsilon_p = 2$. They showed that the precise value of the dielectric constant of protein adopted has only negligible effects on the macroscopic properties derived from simulations. Subsequently, Ng et al. [21] used an adaptive stochastic optimization search algorithm to estimate the optimal ε_p and ε_w for the potassium MthK channel. All possible pairs of ε_w, ranging from 20 to 80 in steps of 10, and ε_p of 2 to 10, in steps of 2, were used to determine which pair gave the least discrepancy between the experimentally-determined current–voltage curve and that obtained from BD simulations. They obtained an optimum value of 2 for the protein dielectric constant and 64 for the pore dielectric constant.

Both of the above methods are self-consistent in that the characteristics, such as ionic conductance, of the channel are replicated. Further work is needed to validate these differing methods using MD simulations. With improved computational facilities it is now possible to do such computations using PMF calculations, but such a calculation is beyond the scope of this paper.

Since few computational studies have been performed on Kir channels, studies such as those presented here provide a useful insight into their conductance properties. Moreover, the crystal structure for Kir3.2 recently became available [2], creating an opportunity to investigate the mechanisms of permeation and rectification using computational tools. Therefore, for the first time, we investigate the mechanisms of ion permeation and inward rectification of the Kir3.2 inwardly rectifying potassium channel using molecular and Brownian dynamics simulations. We ascertain that the Kir3.2 pore is closed by a hydrophobic gating mechanism similar to that observed in the Kv1.2 and acetylcholine receptor channels. This intracellular gate runs from the internal water cavity to the intracellular mouth of the channel ($z = -26$ to -10 Å), and is surrounded by hydrophobic residues. Once open, water floods into the intracellular gate region, and the channel exhibits inward rectification with a conductance of 25 pS at -125 mV in 140 mM symmetric K^+. This compares well with the experimentally determined value of 30 ± 2 pS over the range of -40 to -100 mV [45]. We demonstrate by making the mutation F192E that, contrary to popular belief, inward rectification is not a result of the presence of intracellular cations, but rather the lack of negatively charged residues at the narrow intracellular mouth of the channel. Moreover, rectification can be restored by the addition of intracellular Mg^{2+}.

TPN binds to the extracellular side of the channel with a K_d value of 0.4 μM. We demonstrate that Lys-17 protrudes into the selectivity filter and forms 1.5 ± 0.6 hydrogen bonds with the Tyr-157 of the pore. In addition, we show that Lys21 of the toxin forms a salt bridge with Asp164 of the channel. Our findings agree with work by Jin et al. [47], who found that higher concentrations of TPN-Q were required when the lysine residues in positions 17 and 21 were mutated to alanine.

Acknowledgements

We gratefully acknowledge the support from the Australian Research Council for the Discovery Early Career Researcher Award, and the National Health and Medical Council. Rhys Hawkins from the Visualization Laboratory at the Australian National University and Silvie Ngo provided excellent technical assistance, for which we are grateful. This work was supported by the NCI National Facility at the Australian National University.

References

[1] H. Hibino, A. Inanobe, K. Furutani, S. Murakami, I. Findlay, Y. Kurachi, Inwardly rectifying potassium channels: their structure, function, and physiological roles, Physiol. Rev. 90 (2010) 291–366.
[2] M.R. Whorton, R. MacKinnon, Crystal structure of the mammalian GIRK2 K^+ channel and gating regulation by G proteins, PIP_2, and sodium, Cell 147 (2011) 199–208.
[3] Y. Kubo, J.P. Adelman, D.E. Clapham, L.Y. Jan, A. Karschin, Y. Kurachi, M. Lazdunski, C.G. Nichols, S. Seino, C.A. Vandenberg, International union of pharmacology. LIV. Nomenclature and molecular relationships of inwardly rectifying potassium channels, Pharmacol. Rev. 57 (2005) 509–526.
[4] K.B. Walsh, Targeting GIRK channels for the development of new therapeutic agents, Front. Pharmacol. 2 (2011) 1–8.
[5] C. Neusch, J.H. Weishaupt, M. Bähr, Kir channels in the CNS: emerging new roles and implications for neurological diseases, Cell Tissue Res. 311 (2003) 131–138.
[6] C. Lüscher, P.A. Slesinger, Emerging roles for G protein-gated inwardly rectifying potassium (GIRK) channels in health and disease, Nat. Rev. Neurosci. 11 (2010) 301–315.
[7] F. Reimann, F.M. Ashcroft, Inwardly rectifying potassium channels, Curr. Opin. Cell Biol. 11 (1999) 503–508.
[8] J.M.B. Anumonwo, A.N. Lopatin, Cardiac strong inward rectifier potassium channels, J. Mol. Cell. Cardiol. 48 (2010) 45–54.
[9] M.R. Silver, T.E. DeCoursey, Intrinsic gating of inward rectifier in bovine pulmonary artery endothelial cells in the presence or absence of internal Mg^{2+}, J. Gen. Physiol. 96 (1990) 109–133.
[10] M. Nishida, R. MacKinnon, Structural basis of inward rectification: cytoplasmic pore of the G protein-gated inward rectifier GIRK1 at 1.8 Å resolution, Cell 111 (2002) 957–965.
[11] A. Kuo, J.M. Gulbis, J.F. Antcliff, T. Rahman, E.D. Lowe, J. Zimmer, J. Cuthbertson, F.M. Ashcroft, T. Ezaki, D.A. Doyle, Crystal structure of the potassium channel KirBac1.1 in the closed state, Science 300 (2003) 1922–1926.
[12] T.W. Claydon, S.Y. Makary, K.M. Dibb, M.R. Boyett, The selectivity filter may act as the agonist-activated gate in the G protein-activated Kir3.1/Kir3.4 K^+ channel, J. Biol. Chem. 278 (2003) 50654–50663.
[13] B.A. Yi, Y.F. Lin, Y.N. Jan, L.Y. Jan, Yeast screen for constitutively active mutant G protein-activated potassium channels, Neuron 29 (2001) 657–667.
[14] Y. Ramu, A.M. Klem, Z. Lu, Short variable sequence acquired in evolution enables selective inhibition of various inward-rectifier K^+ channels, Biochemistry 43 (2004) 10701–10709.
[15] H. Kitamura, M. Yokoyama, H. Akita, K. Matsushita, Y. Kurachi, M. Yamada, Tertiapin potently and selectively blocks muscarinic K^+ channels in rabbit cardiac myocytes, J. Pharmacol. Exp. Ther. 293 (2000) 196–205.
[16] S. Haider, S. Khalid, S.J. Tucker, F.M. Ashcroft, M.S.P. Sansom, Molecular dynamics simulations of inwardly rectifying (Kir) potassium channels: a comparative study, Biochemistry 46 (2007) 3643–3652.
[17] C.E. Capener, I.H. Shrivastava, K.M. Ranatunga, L.R. Forrest, G.R. Smith, M.S.P. Sansom, Homology modeling and molecular dynamics simulation studies of an inward rectifier potassium channel, Biophys. J. 78 (2000) 2929–2942.
[18] S.H. Chung, T.W. Allen, S. Kuyucak, Conducting-state properties of the KcsA potassium channels from molecular and Brownian dynamics simulations, Biophys. J. 82 (2002) 628–645.
[19] T.W. Allen, S. Kuyucak, S.H. Chung, Molecular dynamics study of the KcsA potassium channel, Biophys. J. 77 (1999) 2502–2516.
[20] A. Warshel, P.K. Sharma, M. Kato, W.W. Parson, Modeling electrostatic effects in proteins, Biochim. Biophys. Acta 1764 (2006) 1647–1676.
[21] J.A. Ng, T. Vora, V. Krishnamurthy, S.H. Chung, Estimating the dielectric constant of the protein and pore, Eur. Biophys. J. 37 (2008) 213–222.
[22] J.C. Phillips, R. Braun, W. Wang, J. Gumbart, E. Tajkhorshid, E. Villa, C. Chipot, R.D. Skeel, L. Kale, K. Schulten, Scalable molecular dynamics with NAMD, J. Comput. Chem. 26 (2005) 1781–1802.
[23] D. Gordon, S.H. Chung, Permeation and block of the Kv1.2 channel examined using Brownian and molecular dynamics, Biophys. J. 101 (2011) 2671–2678.
[24] M. Hoyles, S. Kuyucak, S.H. Chung, Computer simulation of ion conductance in membrane channels, Phys. Rev. E Stat. Nonlinear Soft Matter Phys. 58 (1998) 3654–3661.
[25] K.M. Ranatunga, I.H. Shrivastava, G.R. Smith, M.S.P. Sansom, Side-chain ionization states in a potassium channel, Biophys. J. 80 (2001) 1210–1219.
[26] A. Burykin, C.N. Schutz, J. Villá, A. Warshel, Simulations of ion current in realistic models of ion channels: the KcsA potassium channel, Proteins 47 (2002) 265–280.
[27] J. Ho, M.L. Coote, First-principles prediction of acidities in the gas and solution phase, WIREs Comput. Mol. Sci. 1 (2011) 649–660.
[28] S.C.L. Kamerlin, M. Haranczyk, A. Warshel, Progress in ab initio QM/MM free-energy simulations of electrostatic energies in proteins: accelerated QM/MM studies of pKa, redox reactions and salvation free energies, J. Phys. Chem. B 113 (2009) 1253–1272.
[29] W. Humphrey, A. Dalke, K. Schulten, VMD: visual molecular dynamics, J. Mol. Graphics 14 (1996) 33–38.
[30] A.D. MacKerell Jr., M. Feig, C.L. Brooks III, Extending the treatment of backbone energetics in protein force fields: limitations of gas-phase quantum mechanics

in reproducing protein conformational distributions in molecular dynamics simulations, J. Comput. Chem. 25 (2004) 1400–1415.
[31] A.D. MacKerell Jr., D. Bashford, M. Bellott, R.L. Dunbrack Jr., J.D. Evanseck, M.J. Field, S. Fischer, J. Gao, H. Guo, S. Ha, D. Joseph-McCarthy, L. Kuchnir, K. Kuczera, F.T.K. Lau, C. Mattos, S. Michnick, T. Ngo, D.T. Nguyen, B. Prodhom, W.E. Reiher III, B. Roux, M. Schlenkrich, J.C. Smith, R. Stote, J. Straub, M. Watanabe, J. Wiorkiewicz-Kuczera, D. Yin, M. Karplus, All-atom empirical potential for molecular modeling and dynamic studies of proteins, J. Phys. Chem. B 102 (1998) 3586–3616.
[32] R. Chen, A. Robinson, D. Gordon, S.H. Chung, Modeling the binding of three toxins to the voltage-gated potassium channel (Kv1.3), Biophys. J. 101 (2011) 2652–2660.
[33] X. Xu, J.W. Nelson, Solution structure of tertiapin determined using nuclear magnetic resonance and distance geometry, Proteins 17 (1993) 124–137.
[34] J. Mintseris, B. Pierce, K. Wiehe, R. Anderson, R. Chen, Z. Weng, Integrating statistical pair potentials into protein complex prediction, Proteins 69 (2007) 511–520.
[35] a) S. Kumar, J.M. Rosenberg, D. Bouzida, R.H. Swendsen, P.A. Kollman, Multidimensional free-energy calculations using the weighted histogram analysis method, J. Comput. Chem. 16 (1995) 1339–1350;
b) A. Grossfield, An implementation of WHAM: the weighted histogram analysis method, http://membrane.urmc.rochester.edu/Software/WHAM/WHAM.html accessed 20 August 2008.
[36] P.C. Chen, S. Kuyucak, Mechanism and energetic of charybdotoxin unbinding from a potassium channel from molecular dynamics simulations, Biophys. J. 96 (2009) 2577–2588.
[37] T.W. Allen, O.S. Andersen, B. Roux, Energetics of ion conduction through the gramicidin channel, Proc. Natl. Acad. Sci. U. S. A. 101 (2004) 117–122.
[38] M.H. Rashid, S. Kuyucak, Affinity and selectivity of ShK toxin for the Kv1 potassium channels from free energy simulations, J. Phys. Chem. B 116 (2012) 4812–4822.
[39] V.B. Luzhkov, F. Österberg, J. Åqvist, Structure-activity relationship for extracellular block by K^+ channels by tetraalkylammonium ions, FEBS Lett. 554 (2003) 159–164.
[40] J. Åqvist, V.B. Luzhkov, B.O. Brandsdal, Ligand binding affinities from MD simulations, Acc. Chem. Res. 35 (2002) 358–365.
[41] M.O. Jensen, D.W. Borhani, K. Lindorff-Larsen, P. Maragakis, V. Jogini, M.P. Eastwood, R.O. Dror, D.E. Shaw, Principles of conduction and hydrophobic gating in K^+ channels, Proc. Natl. Acad. Sci. U. S. A. 107 (2010) 5833–5838.
[42] B. Corry, An energy-efficient gating mechanism in the acetylcholine receptor channel suggested by molecular and Brownian dynamics, Biophys. J. 90 (2006) 799–810.
[43] A. Dryga, S. Chakrabarty, S. Vicatos, A. Warshel, Realistic simulation of the activation of voltage-gated ion channels, Proc. Natl. Acad. Sci. 109 (2012) 3335–3340.
[44] S.H. Chung, B. Corry, Conduction properties of KcsA measured using Brownian dynamics with flexible carbonyl groups in the selectivity filter, Biophys. J. 93 (2007) 44–53.
[45] P. Kofuji, N. Davidson, H.A. Lester, Evidence that neuronal G-protein-gated inwardly rectifying K^+ channels are activated by $G\beta\gamma$ subunits and function as heteromultimers, Proc. Natl. Acad. Sci. U. S. A. 92 (1995) 6542–6546.
[46] S.H. Chung, T.W. Allen, S. Kuyucak, Modeling diverse range of potassium channels with Brownian dynamics, Biophys. J. 83 (2002) 263–277.
[47] W. Jin, A.M. Klem, J.H. Lewis, Z. Lu, Mechanisms of inward-rectifier K^+ channel inhibition by Tertiapin-Q, Biochemistry 38 (1999) 14294–14301.
[48] M.A. Kastenholz, P.H. Hünenberger, Influence of artificial periodicity and ionic strength in molecular dynamics simulations of charged biomolecules employing lattice-sum methods, J. Phys. Chem. B 108 (2004) 774–788.
[49] W. Jin, Z. Lu, Synthesis of a stable form of Tertiapin: a high-affinity inhibitor for inward-rectifier K^+ channels, Biochemistry 38 (1999) 14286–14293.
[50] W. Jin, Z. Lu, A novel high-affinity inhibitor for inward-rectifier K^+ channels, Biochemistry 37 (1998) 13291–13299.
[51] A. Burykin, M. Kato, A. Warshel, Exploring the origin of the selectivity of the KcsA potassium channel, Proteins 52 (2003) 412–426.
[52] C.N. Schutz, A. Warshel, What are the dielectric "constants" of proteins and how to validate electrostatic models? Proteins 44 (2001) 400–417.